Published in IET Power Electronics
Received on 16th December 2008
Revised on 27th January 2010
doi: 10.1049/iet-pel.2008.0344

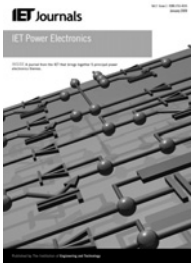

ISSN 1755-4535

Voltage regulation of photovoltaic arrays: small-signal analysis and control design

M.G. Villalva[1] *T.G. de Siqueira*[2] *E. Ruppert*[1]

[1]*School of Electrical and Computer Engineering, University of Campinas – UNICAMP, Campinas – São Paolo, Brazil*
[2]*Department of Engineering, University of Alfenas at Poços de Caldas – UNIFAL, Poços de Caldas – Minas Gerais, Brazil*
E-mail: mvillalva@gmail.com

Abstract: This study deals with the regulation of the output voltage of photovoltaic (PV) arrays. As a case study, the DC–DC buck converter is used as an interface between the PV array and the load, but other types of converters can be used for the same purpose. The input voltage of the converter is controlled in order to regulate the operating point of the array. Besides reducing losses and stress because of the bandwidth-limited regulation of the converter duty cycle, controlling the converter input voltage reduces the settling time and avoids oscillation and overshoot, making easier the functioning of maximum power point tracking (MPPT) methods. The voltage regulation problem is addressed with a detailed analysis that starts with the modelling of the PV array and the converter. This analysis is followed by study, design, simulation and practical experiments of three closed-loop control strategies for the buck converter. Control stability and implementation considerations are presented.

1 Introduction

A photovoltaic (PV) array converts sunlight into electricity. The voltage and current available at the terminals of the PV array may directly feed small loads such as lighting systems and DC motors. More sophisticated applications require electronic converters to process the electricity from the array. These converters may be used to regulate the voltage and current at the load, to control the power flow in grid-connected systems and mainly to track the maximum power point (MPP) of the array.

Converters with the maximum power point tracking (MPPT) feature use an algorithm to continuously detect the maximum instantaneous power of the PV array. As the operating conditions of the array (solar irradiation and temperature) may change randomly during the operation of the system, an MPPT algorithm is necessary so that the maximum instantaneous power can be extracted and delivered to the load.

Many MPPT methods have been proposed in the literature. Many theoretical improvements and even advanced techniques of artificial intelligence have been proposed to enhance MPPT methods in order to obtain performance improvements. However, the achievement of MPPT strongly depends on the performance of the converter control and its ability to regulate the operating point of the PV array.

The PV array operating point can be adjusted by regulating the voltage or current at the terminals of the array. The voltage control is preferred because the voltage at the MPP is approximately constant [1]. The PV current, on the other hand, changes greatly when the solar irradiation varies.

This paper addresses the control problem illustrated in Fig. 1. The PV array feeds the DC–DC buck converter. The output of the converter is represented by a constant DC voltage source V_o that represents a battery or a DC link for another cascaded converter. The buck converter serves as an interface between the PV array and the voltage V_o. The MPPT block (not studied in this paper) provides a voltage reference and the voltage controller regulates the PV array voltage.

Some works in the literature present PV systems with the direct duty cycle control of the DC–DC converter [2–4], where the MPPT block directly actuates on the converter

© The Institution of Engineering and Technology 2010

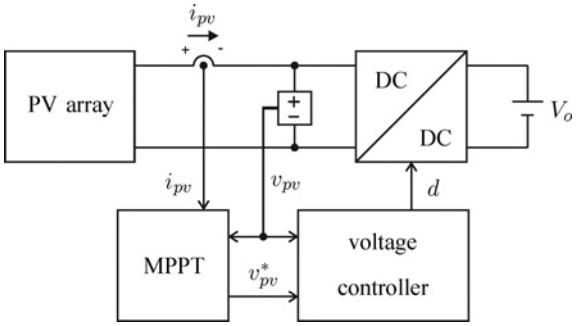

Figure 1 *Input-regulated converter interfaces the PV array with the output V_o, which may be a battery or a cascaded converter*

duty cycle without employing a voltage or current controller. In this kind of system, no appropriate voltage or current regulation is achieved and the converter is subject to increased switching stress and losses [5]. A feedback controller with a proportional and integral (PI) compensator for regulating the converter voltage is preferred. Besides reducing losses and stress due to the bandwidth-limited regulation of the duty cycle, the presence of the controller reduces the settling time of the converter and avoids oscillation and overshoot, making easier the functioning of MPPT methods [6].

2 PV array modelling

Photovoltaic devices present the non-linear $i \times v$ characteristic illustrated in Fig. 2. This example shows the curve of the KC200GT [7] solar array.

The equation of the $i \times v$ characteristic is [8, 9]

$$i_{\mathrm{pv}} = I_{\mathrm{pv}} - I_0\left[\exp\left(\frac{v_{\mathrm{pv}} + R_{\mathrm{s}} i_{\mathrm{pv}}}{V_{\mathrm{t}} a}\right) - 1\right] - \frac{v_{\mathrm{pv}} + R_{\mathrm{s}} i_{\mathrm{pv}}}{R_{\mathrm{p}}} \quad (1)$$

where I_{pv} and I_0 are the photovoltaic and saturation currents

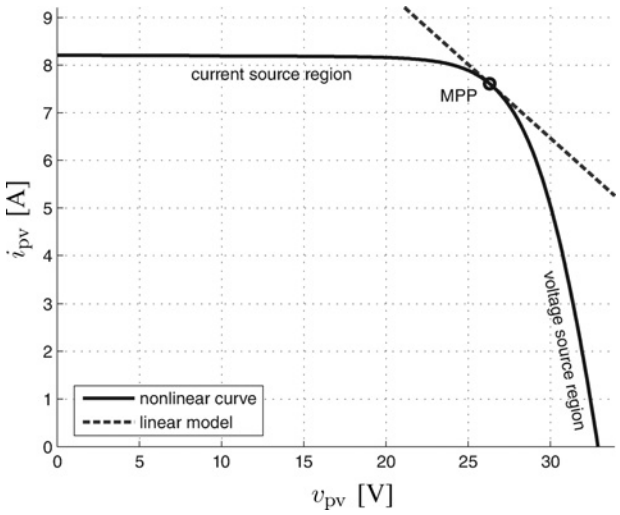

Figure 2 *Non-linear i × v characteristic of the KC200GT solar array and equivalent linear model at the MPP*

of the array, $V_{\mathrm{t}} = N_{\mathrm{s}} kT/q$ is the thermal voltage with N_{s} cells connected in series (k is the Boltzmann constant, q is the electron charge and T is the temperature of the PV cells), R_{s} is the equivalent series resistance, R_{p} is the equivalent shunt resistance and a is the ideality constant of the diode. The parameters of (1) may be obtained from practical measured characteristics of the PV array. An explanation on the PV array modelling and the determination of the parameters of the $i \times v$ equation may be found in [8, 9].

A linear PV array model is necessary in the analyses that will be done in the next sections. The nominal $i \times v$ curve is linearised at the MPP as shown in Fig. 2.

The derivative of the non-linear $i \times v$ curve at a given point (V, I) is

$$g(V, I) = -\frac{I_0}{V_{\mathrm{t}} N_{\mathrm{s}} a} \exp\left(\frac{V + IR_{\mathrm{s}}}{V_{\mathrm{t}} N_{\mathrm{s}}}\right) - \frac{1}{R_{\mathrm{p}}} \quad (2)$$

The linear model is described by the line tangent to the $i \times v$ curve at the linearisation point (V, I)

$$i_{\mathrm{pv}} = (-gV + I) + g v_{\mathrm{pv}} \quad (3)$$

and may be represented by the equivalent circuit of Fig. 3, where $R_{\mathrm{eq}} = -1/g$ and $V_{\mathrm{eq}} = V - I/g$.

The circuit of Fig. 3 is valid at the linearisation point (V, I) and is a good approximation of the PV array for a small-signal analysis at the vicinities of this point. The dynamic behaviour of the system composed of the PV array and buck converter depends strongly on the point of operation of the array. The system is designed and optimised to operate at the MPP and later the design is checked for

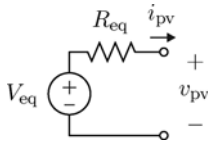

Figure 3 *Linear equivalent circuit valid at the linearisation point*

Table 1 Parameters of the KC200GT solar array

I_0	9.825×10^{-8} A
I_{pv}	8.214 A
a	1.3
R_{p}	415.405 Ω
R_{s}	0.221 Ω
V_{eq}	50.9007 V
R_{eq}	3.2327 Ω

© The Institution of Engineering and Technology 2010

doi: 10.1049/iet-pel.2008.0344

other operating points. The operation in the current source region of the $i \times v$ curve (see Fig. 2) presents the worst and most critical dynamic behaviour [1, 10]. In a later section, several closed-loop configurations will be analysed and they will be evaluated in all regions of the $i \times v$ curve.

Table 1 lists the parameters of the KC200GT array obtained through modelling [8, 9].

3 Converter modelling

In this section, small-signal models of the buck converter fed by the PV array are developed. The method of average variables [11–14] is used to obtain small-signal converter transfer functions. The first and second models describe the behaviour of v_{pv} and i_L with respect to the duty cycle of the converter. The third model describes the behaviour of v_{pv} with respect to i_L.

3.1 Average state equations

Fig. 4 shows the PV-buck system with average voltages and currents. The bar over a variable name (e.g. $\bar{v}$, $\bar{i}$) means the discrete-time average value of the variable within one switching period of the converter. By writing the circuit equations with average variables, the high-frequency components are eliminated and only the natural system behaviour remains.

The average capacitor state equation is

$$\frac{V_{eq} - \bar{v}_{pv}}{R_{eq}} - C\frac{d}{dt}\bar{v}_C - \bar{i}_1 = 0 \tag{4}$$

The average inductor state equation is

$$\bar{v}_{34} - R_L\bar{i}_L - V_o - L\frac{d}{dt}\bar{i}_L = 0 \tag{5}$$

The circuit constituting the transistor and diode may be replaced by the average equivalent quadripole with terminals 1–2–3–4, which is described by the following equations, where d is the duty cycle of the transistor

$$\bar{v}_{34} = \bar{v}_{12}d = \bar{v}_{pv}d \tag{6}$$

$$\bar{i}_1 = \bar{i}_3 d = \bar{i}_L d \tag{7}$$

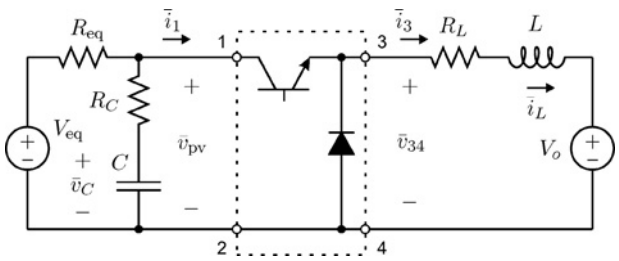

Figure 4 *Buck converter with PV array linear model*

Finally, the following equation relates the input voltage of the converter and the capacitor voltage

$$\bar{v}_{pv} = R_C\frac{d}{dt}\bar{v}_C + \bar{v}_C \tag{8}$$

3.2 Small-signal model for voltage control

The objective of modelling the converter for voltage control is to obtain a small-signal transfer function that relates the small-signal voltage $\hat{v}_{pv}$ and the control variable $\hat{d}' = -\hat{d}$. The minus signal is necessary because negative variations of duty cycle cause positive increments in the input voltage.

The modelling process is essentially composed of three steps: inserting the small-signal variables in the state equations, applying the Laplace transformation and manipulating the equations in order to find the desired transfer function.

The small-signal variables are introduced with the following definitions

$$\begin{aligned} \bar{v}_C &= V_C + \hat{v}_C \\ \bar{v}_{pv} &= V_{pv} + \hat{v}_{pv} \\ \bar{i}_L &= I_L + \hat{i}_L \\ d &= D - \hat{d} \end{aligned} \tag{9}$$

where DC steady state values are capitalised and small signals are marked with a hat.

By substituting (7) and (8) in (4) and then replacing the average variables by the definitions of (9) one finds

$$\begin{aligned} &I_L\hat{d} + \hat{d}\hat{i}_L + V_C/R_{eq} + V_{eq}/R_{eq} - \hat{v}_C/R_{eq} - I_L D - \\ &\quad - \hat{i}_L D - C\frac{d}{dt}\hat{v}_C - R_C C/R_{eq}\frac{d}{dt}\hat{v}_C = 0 \end{aligned} \tag{10}$$

From (10), by neglecting the non-linear product $\hat{d}\hat{i}_L$ and applying the Laplace transformation, the small-signal equation is obtained

$$\begin{aligned} &I_L\hat{d}(s) - \hat{v}_C(s)/R_{eq} - \\ &\quad - \hat{i}_L(s)D - sC\hat{v}_C(s) - sR_C C/R_{eq}\hat{v}_C(s) = 0 \end{aligned} \tag{11}$$

Similarly, from (5), (6), (8) and (9), one gets

$$\begin{aligned} &-V_C\hat{d}(s) - R_L\hat{i}_L(s) + \hat{v}_C(s)D - R_C C V_C s\hat{d}(s) + \\ &\quad + R_C C D s\hat{v}_C(s) - sL\hat{i}_L(s) = 0 \end{aligned} \tag{12}$$

From (11), (12) and (8) one gets the voltage to duty cycle

© The Institution of Engineering and Technology 2010

transfer function

$$G_{vd}(s) = \hat{v}_{pv}/\hat{d}'(s) = \frac{(1+sCR_C)(I_L + (VD(1-sCR_C))/(R_L+sL))}{sC + (1+sCR_C)((1/R_{eq}) + (D^2/(R_L+sL)))} \quad (13)$$

3.3 Small-signal model for current control

The objective of modelling the converter for current control is to obtain a small-signal transfer function that relates the buck converter inductor current i_L and the converter duty cycle. One must notice that in this case, unlike the voltage transfer function previously obtained, the control variable is $\hat{d}$ because positive duty cycle increments cause positive current increments.

The modelling process has the same steps used in the previous section, so the development of the inductor current transfer function will not be presented in detail. For the current control, the following definitions are used

$$\begin{aligned} \bar{v}_C &= V_C + \hat{v}_C \\ \bar{v}_{pv} &= V_{pv} + \hat{v}_{pv} \\ \bar{i}_L &= I_L + \hat{i}_L \\ d &= D + \hat{d} \end{aligned} \quad (14)$$

From the average state equations (4) and (5), with (8) and (14), the following current to duty cycle transfer function is obtained

$$G_{id}(s) = \hat{i}_L(s)/\hat{d}(s) = \left(\frac{I_L D}{sC(1+(R_C/R_{eq})) + (1/R_{eq})} - V\right)(1+sCR_C)/\left(-R_L - sL - \frac{D^2(1+sCR_C)}{sC(1+(R_C/R_{eq})) + (1/R_{eq})}\right) \quad (15)$$

3.4 Small-signal model for voltage and current control

The objective of modelling the converter for voltage and current control is to obtain a transfer function that relates the input voltage $\hat{v}_{pv}$ to the inductor current $\hat{i}_L$. This transfer function will be used in the double-loop control scheme presented later, where both the current and the voltage of the converter are controlled. In this scheme, the control variable of $\hat{i}_L$ is the duty cycle $\hat{d}$ and the control variable of $\hat{v}_{pv}$ is $\hat{i}'_L = -\hat{i}_L$.

The $\hat{v}_{pv}(s)/\hat{i}'_L(s)$ transfer function is obtained by assuming that small duty cycle perturbations directly affect the current $\hat{i}_L$ and the dynamics of $\hat{v}_C$ is dictated by $\hat{i}_L$. In this way, $\hat{v}_C$ is decoupled from $\hat{d}$ and this permits to easily obtain a very useful transfer function for $\hat{v}_{pv}$. The influence of $\hat{d}$ on the system is already embedded in the $\hat{i}_L(s)/\hat{d}(s)$ transfer function and the system is analysed near the operating point corresponding to the steady-state duty cycle D, so one can make $\bar{i}_1 = \bar{i}_L D$ as shown in the circuit of Fig. 5.

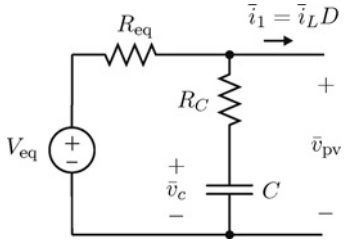

Figure 5 *Equivalent average circuit used to obtain $G_{vi}(s)$*

$$\frac{V_{eq} - \bar{v}_{pv}}{R_{eq}} - C\frac{d}{dt}\bar{v}_C - \bar{i}_L D = 0 \quad (16)$$

By using (8) and (16) with the following small-signal definitions

$$\begin{aligned} \bar{v}_C &= V_C + \hat{v}_C \\ \bar{v}_{pv} &= V_{pv} + \hat{v}_{pv} \\ \bar{i}_L &= I_L - \hat{i}_L \\ d &= D + \hat{d} \end{aligned} \quad (17)$$

the desired transfer function is found

$$G_{vi}(s) = \frac{\hat{v}_{pv}(s)}{\hat{i}'_L(s)} = \frac{D(1+sCR_C)R_{eq}}{1 + sCR_C + sCR_C R_{eq}} \quad (18)$$

4 Open-loop analysis

With the converter transfer functions $G_{vd}(s)$, $G_{id}(s)$ and $G_{vi}(s)$, one can make some analyses of the PV-buck system that help understand the effects of R_L and R_C in the system. Before these analyses are done, the transfer functions are validated by comparison with the responses of a simulated switching converter built with the parameters of Tables 1 and 2.

4.1 Validation of transfer functions

Figs. 6–8 show simulation results of the buck converter and the transfer functions. The converter switching frequency is 20 kHz and the circuit was evaluated with the PSIM simulator. The responses of the switching converter are superimposed with the transfer function responses so that one can verify the validity of the small-signal modelling in the time domain. The responses match almost perfectly and the results are reasonably good considering the simplifications and assumptions made in the mathematical modelling.

© The Institution of Engineering and Technology 2010

doi: 10.1049/iet-pel.2008.0344

Table 2 Characteristics of the buck converter

L	2 mH
R_L	0.1 Ω
C	3000 μF
R_C	0.05 Ω
V_o	13.15 V
D	0.5

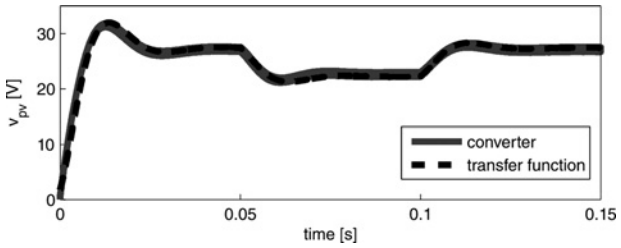

Figure 6 *Simulated converter and $G_{vd}(s)$ transfer function responses to small-signal steps around the operating point $D = 0.5$*

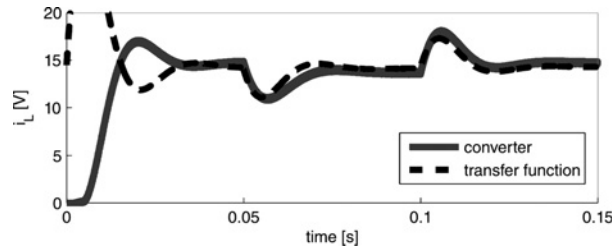

Figure 7 *Simulated converter and $G_{id}(s)$ transfer function responses to small-signal steps around the operating point $D = 0.5$*

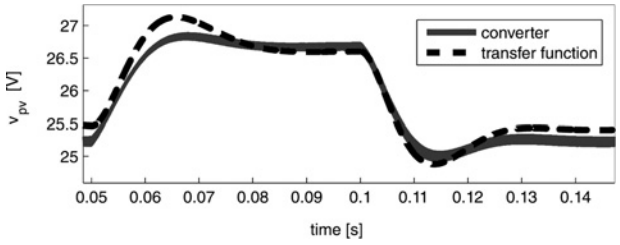

Figure 8 *Simulated converter and $G_{vi}(s)$ transfer function responses to small-signal steps around the operating point $D = 0.5$*

Figs. 9–11 show frequency responses of the switching converter obtained with the ACSWEEP analysis from 10 Hz to 10 kHz. The responses are superimposed on the same axes with the responses of the transfer functions $G_{vd}(s)$, $G_{id}(s)$ and $G_{vi}(s)$.

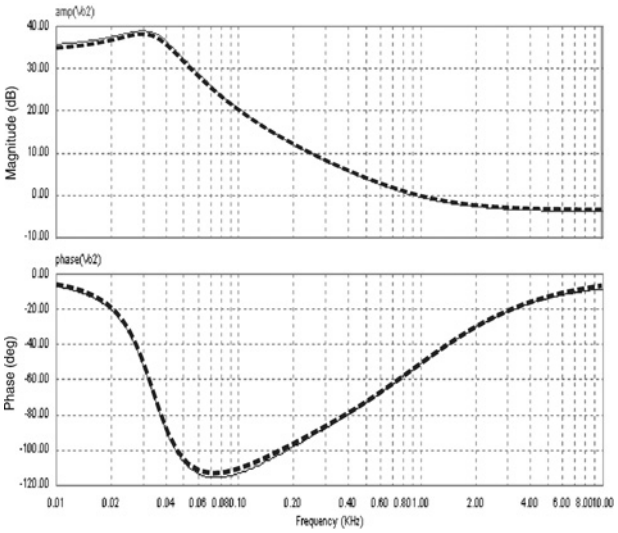

Figure 9 *Bode plots of the simulated converter frequency response and the transfer function $G_{vd}(s)$ (dashed line) superimposed*

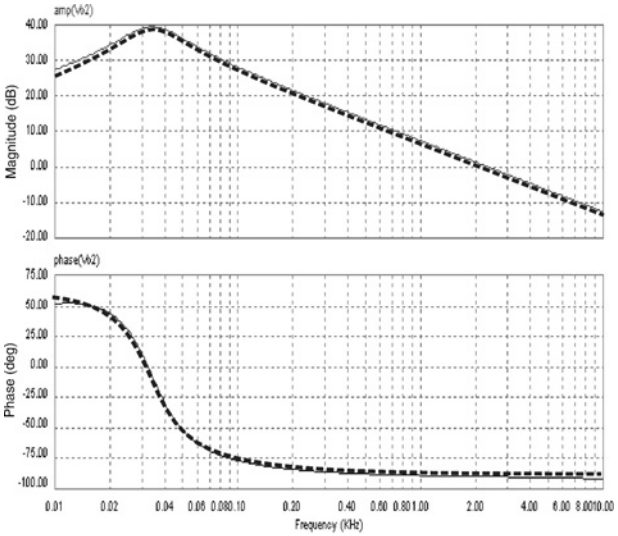

Figure 10 *Bode plots of the simulated converter frequency response and the transfer function $G_{id}(s)$ (dashed line) superimposed*

The comparison of the time- and frequency-domain responses of the converter and the transfer functions confirms that the small-signal modelling procedure is correct and the model transfer functions can be used to analyse the converter and design closed-loop systems.

4.2 Influence of R_C and R_L

In [1, 15] the problem of PV voltage regulation was addressed with a boost converter using simplified converter models, where only R_L is considered and R_C is neglected. However, both R_C and R_L are important parameters that must be considered in the model if one wishes for a

© The Institution of Engineering and Technology 2010

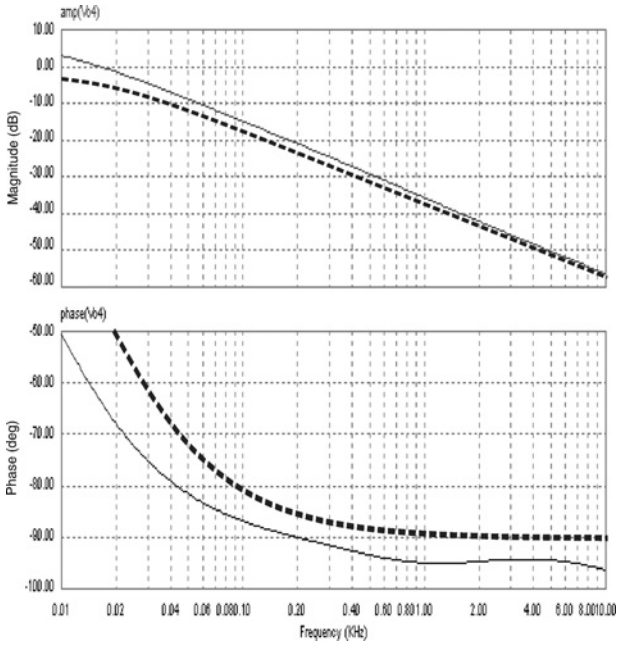

Figure 11 *Bode plots of the simulated converter frequency response and the transfer function $G_{vi}(s)$ (dashed line) superimposed*

realistic and useful analysis of the input-regulated DC–DC converter fed by a PV array.

Figs. 12 and 13 illustrate the effects of R_C and R_L on the system responses. Fig. 13 shows that R_L dumps the system and makes it more stable. No noticeable effect of R_C is present in the responses of Fig. 13, but in Fig. 12 one notices that R_C introduces a high-frequency zero in the system and reduces the system phase lag.

Although R_C is generally undesired in converter designs, in the input-regulated converter it helps to stabilise the system by increasing the phase margin and significantly reducing the phase lag at high frequencies. This explains why even a poorly designed compensator may work with

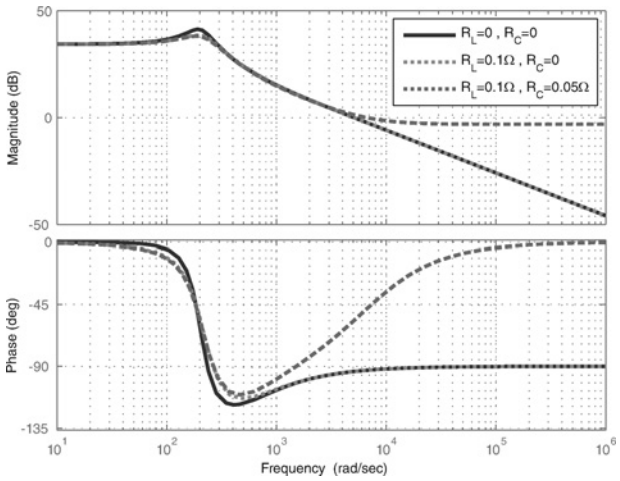

Figure 12 *Bode responses of $G_{vd}(s)$ for different R_C and R_L*

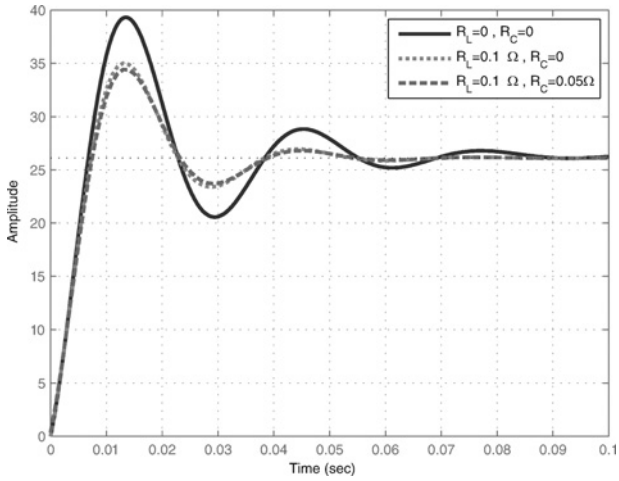

Figure 13 *Step responses of $G_{vd}(s)$ for different R_C and R_L*

this kind of system. Neglecting R_C produces a wrong converter model that leads to wrong conclusions and wrong compensator design. Generally, because of the abrupt and large phase shift observed in the Bode plots of the input-regulated converter, the compensator design is considered difficult and a second-order proportional integral derivative (PID) compensator is suggested in some works [1, 15]. However, an ordinary PI compensator must be enough to regulate the PV array voltage if R_C is considered in the model.

5 Closed-loop design

The design of closed-loop controllers for the DC–DC converter fed by a PV array is based on the transfer functions developed in previous sections. In the following subsections, three control strategies for the buck converter will be studied theoretically and experimentally. The two last subsections make brief analyses about the practical implementation of the compensators and about the stability of the closed-loop systems when the operating point of the PV array changes. An experimental converter with the parameters presented in Table 2 was built and evaluated.

5.1 Single feedback loop voltage controller

In the single-loop scheme of Fig. 14, the voltage controller actuates on the converter duty cycle and directly regulates the input voltage v_{pv}. Fig. 15 shows how the controller is constituted.

Fig. 16 shows the Bode plots of $G_{vd}(s)$ (open-loop system) and of the loop transfer function $C_{vd}(s)H_vG_{vd}(s)$ (compensated system). The system is compensated with $C_{vd}(s) = (30s + 750)/s$ and the feedback gain is $H_v = 1/30$. The compensator places the crossover frequency at $\omega = 6.6 \times 10^3$ rad/s. As a rule of thumb, the crossover frequency can be chosen to be equal or greater than the break frequency of the zero $(1 + sCR_C)$, $\omega = 1/(CR_C)$, thus avoiding the critical phase-shift zone

© The Institution of Engineering and Technology 2010

doi: 10.1049/iet-pel.2008.0344

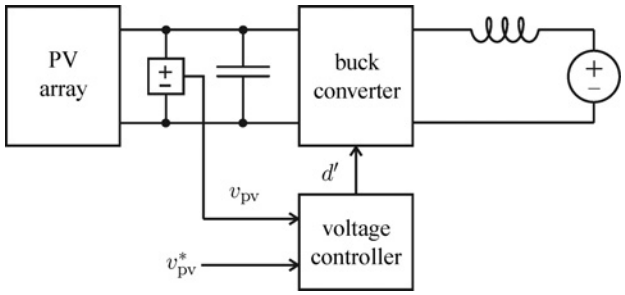

Figure 14 *Voltage-controlled converter*

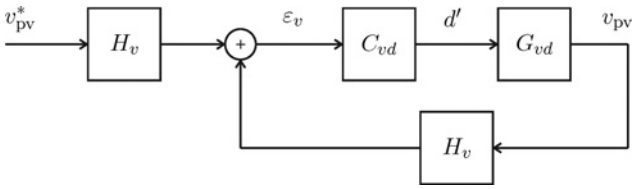

Figure 15 *Voltage controller with single feedback loop*

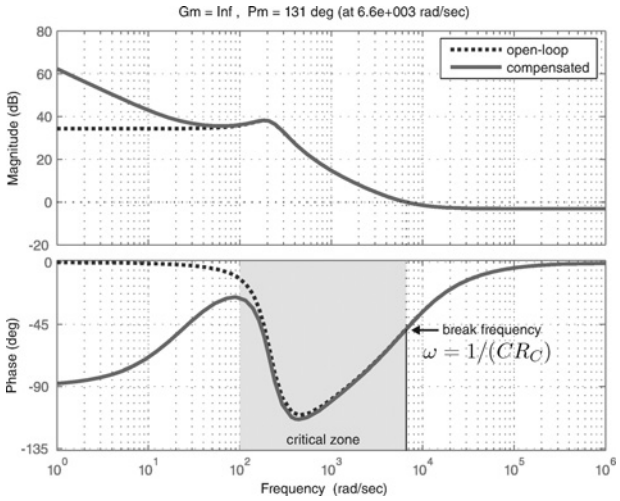

Figure 16 *Bode plots of the open-loop system $G_{vd}(s)$ and the compensated system $C_{vd}(s)H_vG_{vd}(s)$*

highlighted in Fig. 16. This warranties good phase margin even when the PV array operates at points other than the point at which the $i \times v$ curve was linearised. Fig. 17 shows an experimental result of the converter with the single-loop voltage controller.

5.2 Double feedback loop voltage controller

In the double-loop scheme of Fig. 18, the converter inductor current is directly controlled and the input voltage is indirectly regulated. The voltage controller generates a current reference for the current controller and the current controller actuates on the converter duty cycle and regulates the inductor current.

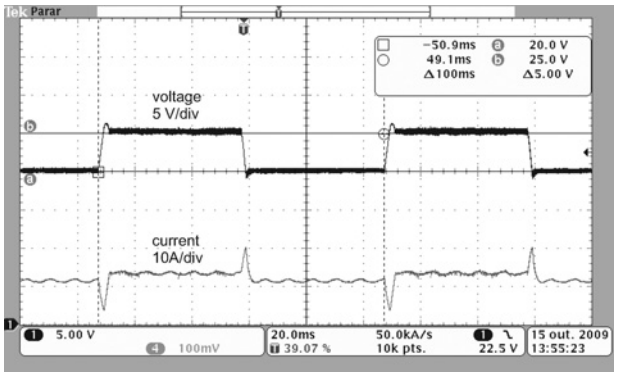

Figure 17 *Experimental result with the single-loop voltage controller: regulated input voltage and inductor current ($v^*_{pv} = 20$ and 25 V)*

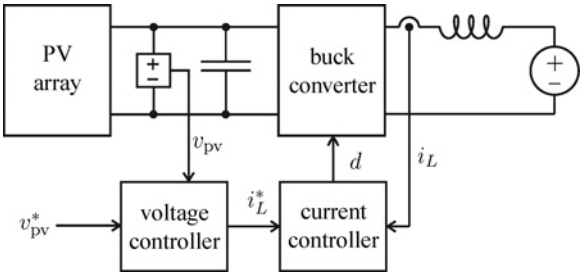

Figure 18 *Voltage- and current-controlled converter*

5.2.1 Current control loop: Fig. 19 shows how the current controller is constituted. Fig. 20 shows the loop Bode plots of the uncompensated and compensated systems. In this example, the system is compensated with $C_{id}(s) = (9.5s + 950)/s$. The crossover frequency is placed at 1 kHz and the phase margin is 90°. Fig. 21 shows an experimental result of the current controller.

5.2.2 Voltage control loop: Fig. 22 shows the control scheme employing an inner current control loop and an external voltage loop. The closed-loop current controller transfer function is

$$G_{icl}(s) = \frac{C_{id}(s)G_{id}(s)}{1 + C_{id}(s)G_{id}(s)H_i} \tag{19}$$

With the transfer functions $G_{icl}(s)$ and $G_{vi}(s)$ from (19) and (15), the compensator $C_{vi}(s)$ may be designed in order to control the input voltage v_{pv}.

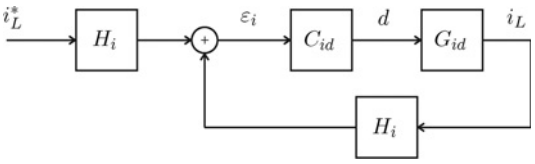

Figure 19 *Current controller*

© The Institution of Engineering and Technology 2010

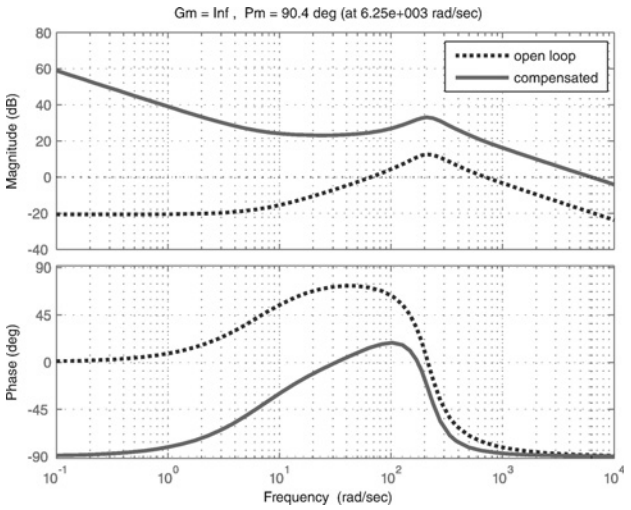

Figure 20 *Bode plots of the open-loop transfer function $G_{id}(s)$ and the compensated system $C_{id}(s)H_iG_{id}(s)$*

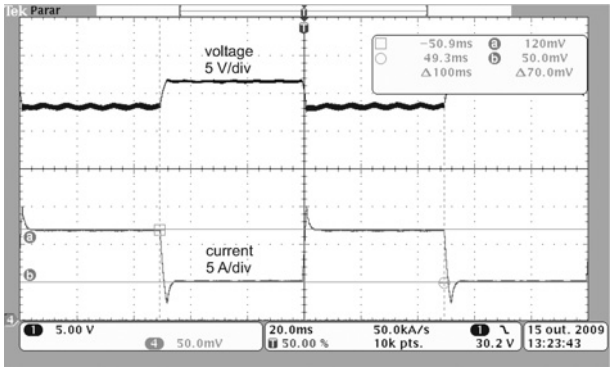

Figure 21 *Experimental result with current controller: input voltage and controlled inductor current ($i_L^* = 5$ and 12 A)*
In this example only the inductor current is controlled

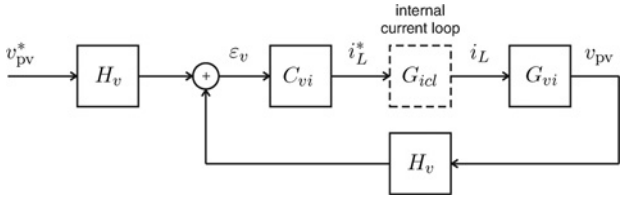

Figure 22 *Voltage control with internal current control loop*

Fig. 23 shows the Bode plots of the uncompensated loop transfer function $G_{icl}(s)G_{vi}(s)H_v$ and of the system compensated with $C_{vi}(s) = (32s + 3200)/s$. Owing to the 180° phase shift some care must be taken when placing the crossover frequency. In this example, the compensated system bandwidth was chosen to be 500 Hz and the phase margin is 63.8°. If a greater bandwidth is desired, a derivative compensator may be necessary to boost the phase margin at the crossover frequency.

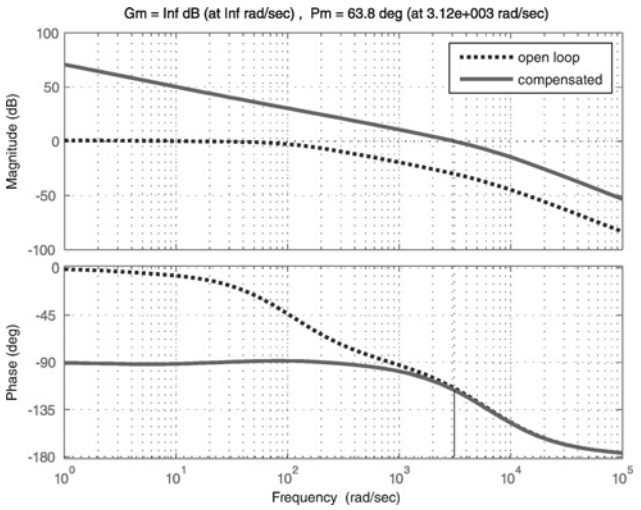

Figure 23 *Voltage control with inner current loop: Bode plots of the uncompensated and compensated loop transfer functions*

Fig. 24 shows an experimental result with the double-loop control scheme. Both current and voltage are controlled. The major advantage of this control scheme is that the inductor current may be controlled (and limited) in order to avoid current overshoots that may be potentially dangerous when large voltage steps occur.

5.3 Digital compensators

The continuous-time compensators designed in previous sections can be realised as discrete-time digital compensators. There are several ways of discretising analogue compensators. All of them present similar results when the compensator bandwidth is not greater than 10% of the sampling frequency [16]. The Tustin or bilinear transformation is used in this work. The compensators and controllers were implemented with the Texas floating point digital signal controller TMS320F28335 with sampling frequency $f_s = 1/T_s = 10$ kHz.

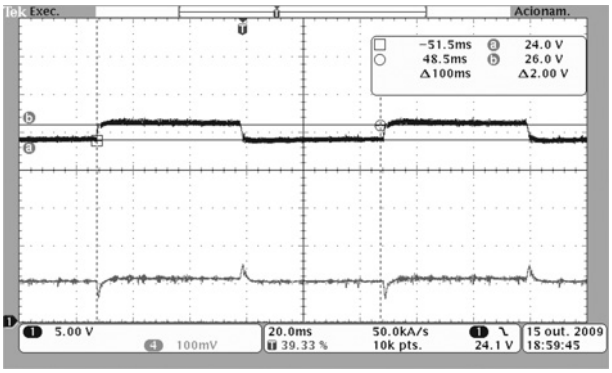

Figure 24 *Experimental result with double-loop controller: controlled input voltage ($v_{pv}^* = 24$ and 26 V) and controlled inductor current*

© The Institution of Engineering and Technology 2010

doi: 10.1049/iet-pel.2008.0344

A discrete-time compensator is a digital filter. The filter coefficients may be obtained from the s-domain transfer function with the desired transformation method. In MATLAB the following command may be used to find the filter coefficients: `[numz, denz] = bilinear (nums, dens, fs)`, where `numz = [b0 b1]` and `denz = [a0 a1]` are the numerator and denominator vectors with the coefficients of the Tustin (or bilinear) approximation.

In the infinite impulse response (IIR) direct transposed form, the filter difference equation is [17]

$$y_k = b_0 e_k + b_1 e_{k-1} - a_1 y_{k-1} \tag{20}$$

where y is the compensator output and e is the control error.

The difference equation (20) is the simplest way to implement the PI compensator. The proportional and integral components are embedded in the equation. In order to implement the simple anti-windup strategy proposed in this paper, one wishes to develop another equation.

The following equation describes a PI compensator

$$y_k = K_p e_k + K_i i_k \tag{21}$$

with the trapezoidal integrator i_k

$$i_k = \frac{T_s}{2}[e_k + e_{k-1}] + i_{k-1} \tag{22}$$

The compensator of (21) and (22) is equivalent to the compensator described by (20), with the difference that in (21) the proportional and integral parts are separated.

One can write the past integrator value i_{k-1} as

$$i_{k-1} = \frac{1}{K_i} y_{k-1} - \frac{K_p}{K_i} e_{k-1} \tag{23}$$

so i_k can be rewritten as

$$i_k = \frac{T_s}{2} e_k + \frac{T_s}{2} e_{k-1} + \frac{1}{K_i} y_{k-1} - \frac{K_p}{K_i} e_{k-1} \tag{24}$$

Replacing (24) in (21), the difference equation (20) becomes

$$y_k = \underbrace{\left[K_p + \frac{k_i T_s}{2}\right]}_{b_0} e_k + \underbrace{\left[\frac{K_i T_s}{2} - K_p\right]}_{b_1} e_{k-1} + y_{k-1} \tag{25}$$

Equation (25) shows the correspondence between the coefficients of (21) and (20), with $a_1 = -1$. Equations (20) and (21) may be used indistinctly to implement

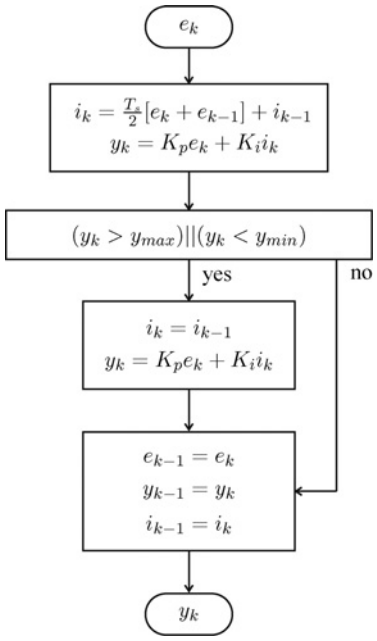

Figure 25 *PI compensator with integrator anti-windup action*

the first-order PI compensator. However, in the form of (21), the simple anti-windup algorithm of Fig. 25 is possible. This algorithm simply stops the integrator when the control output exceeds the limits. In practical systems, the compensator output may sometimes exceed the maximum effective control effort. This causes integrator saturation and deteriorates the control performance.

Fig. 26 shows a simulation result employing a voltage compensator with the proposed anti-windup scheme. The simulated system is the double-loop voltage control of Fig. 22. In contrast, Fig. 27 shows the same system controlled with a conventional compensator without integrator anti-windup action.

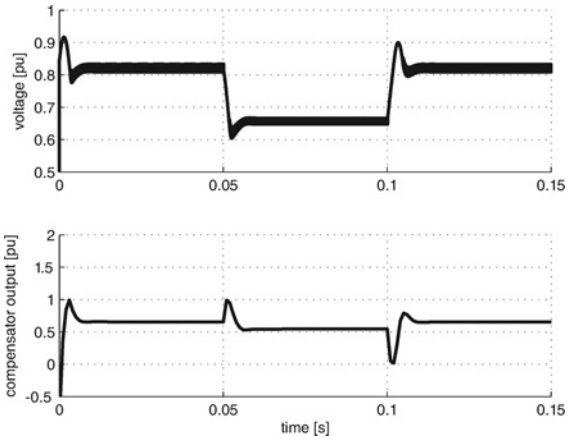

Figure 26 *Controlled voltage and compensator output with integrator anti-windup action*

© The Institution of Engineering and Technology 2010

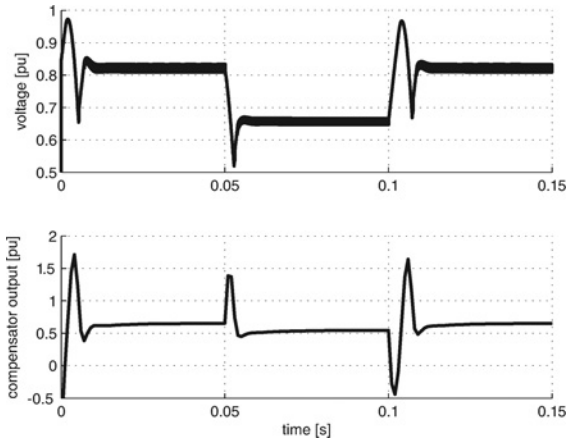

Figure 27 *Controlled voltage and compensator output without integrator anti-windup action*

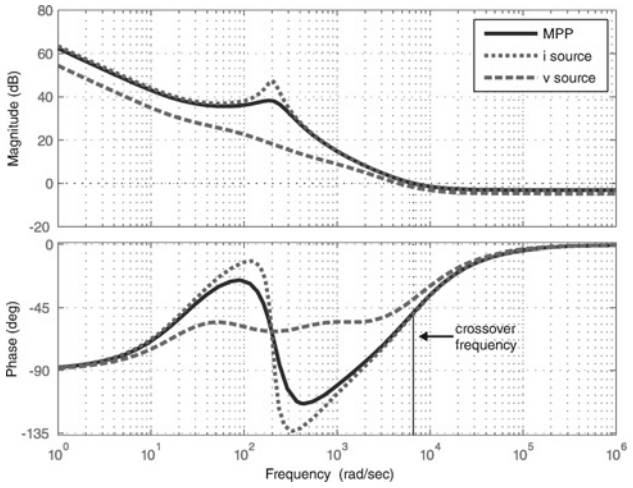

Figure 28 *Single-loop voltage control: Bode plots of the closed-loop system compensated with $C_{vd}(s)$ in three different operating points of the PV array $i \times v$ curve*

5.4 Stability analysis

At the beginning of the analysis, the PV array was linearised at the nominal MPP and the closed-loop system was designed to operate at the vicinities of this point. Although the system is ideally optimised to operate at the nominal MPP, the closed-loop system can work satisfactorily at other operating points also. This can be verified through simulation and experimentally. From the theoretical point of view, the most important concern is the stability analysis. Although the closed-loop system is not expected to present the same performance when the operating point moves along the $i \times v$ curve (and when the $i \times v$ curve itself changes), the system must be stable independently of the conditions.

It was shown in [10] that when the operating point of the PV array moves towards the voltage source region of the $i \times v$ curve, the system becomes more dumped and stable. On the other hand, when the operating point moves leftward and enters the current source region of the $i \times v$ curve, the dynamic behaviour of the system is more critical. Even considering that the system operates at the MPP, the system dynamics becomes less or more critical when the temperature or the solar irradiation changes. An in-depth analysis of the dynamic behaviour of the PV-buck system in different points of the $i \times v$ curve is beyond the objectives of this paper. However, in Figs. 28–30 one can observe the Bode responses of the closed-loop system when operating in the extreme edges of the current-source and voltage-source regions of the $i \times v$ curve. The operation in the current-source region demonstrated in these figures correspond to the worst-case operation of the PV-buck system. The comparisons provided by these figures show that if the closed-loop crossover frequency is sufficiently high, the displacement of the PV array operating point has no impact on the system stability. As seen in Figs. 28–30, above the crossover frequencies the gain and phase characteristics of the systems are approximately the same. The only exception is for the operation in the voltage source region, which makes the system more stable due to the increased phase margin in Figs. 28 and 30.

The conclusion is that placing the closed-loop crossover frequency sufficiently far from the critical phase-shift zone is enough to warranty the system operation at all points of the $i \times v$ curve. Regarding the operation of the PV array with conditions different of the nominal ones, it may be shown (this is the subject of a future paper) that changing the temperature and solar irradiation produces the same effect, from the point of view of the converter dynamic analysis, as moving the operating point along the nominal $i \times v$ curve. In fact, what matters is the punctual conductance of the $i \times v$ curve at the point of operation. Changing the $i \times v$ curve or moving the operating point

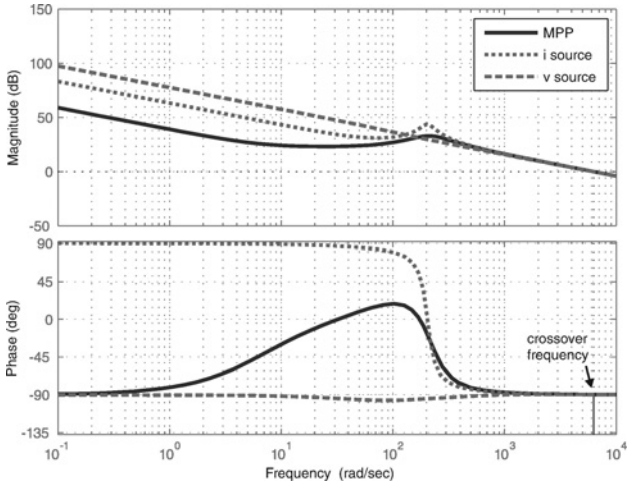

Figure 29 *Single-loop current control: Bode plots of the closed-loop system compensated with $C_{id}(s)$ in three different operating points of the PV array $i \times v$ curve*

© The Institution of Engineering and Technology 2010

doi: 10.1049/iet-pel.2008.0344

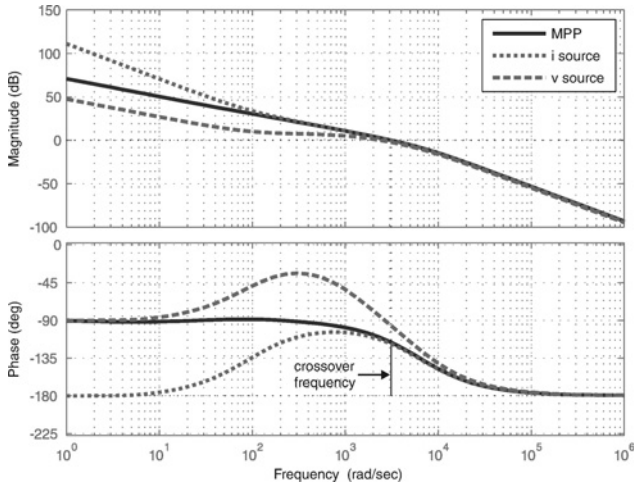

Figure 30 *Double-loop voltage control: Bode plots of the closed-loop system compensated with $C_{vi}(s)$ in three different operating points of the PV array $i \times v$ curve*

to the worst place (i.e. to the extremity of the current source region) corresponds to the situations analysed in Figs. 28–30.

6 Conclusions

Regulation of photovoltaic voltage can be achieved with ordinary PI compensators. Although the literature shows many examples of uncompensated converters, controlling the output voltage of a PV device brings the advantage of significantly increasing the performance of MPPT algorithms [6]. This paper has presented a detailed analysis of the PV voltage regulation problem using a buck converter as a PV array interface. The analysis permits the solid design (with compensator design criteria) of the control systems. Three control strategies were proposed and investigated. The controllers were optimised to operate at the nominal MPP of the PV device. The reasons for this choice were explained in Section 2, where the modelling of the PV device was presented. In Section 3 the converter and the PV array were modelled and system transfer functions were developed. In Section 4, the closed-loop systems were analysed theoretically and experimentally and a brief consideration about the discrete-time implementation of PI compensators was presented. Finally, Section 4 presented some considerations regarding the closed-loop system stability.

7 Acknowledgments

This work was financially supported by FAPESP and CNPq. Evaluation boards kindly donated by Texas Instruments were used in the research.

8 References

[1] XIAO W., DUNFORD W.G., PALMER P.R., CAPEL A.: 'Regulation of photovoltaic voltage', *IEEE Trans. Ind. Electron.*, 2007, **54**, (3), pp. 1365–1374

[2] FEMIA N., PETRONE G., SPAGNUOLO G., VITELLI M.: 'Optimizing duty-cycle perturbation of P&O MPPT technique'. Power Electronics Specialists Conf., 2004, PESC 04, 2004 IEEE 35th Annual, 2004, vol. 3, pp. 1939–1944

[3] FEMIA N., PETRONE G., SPAGNUOLO G., VITELLI M.: 'Optimizing sampling rate of P&O MPPT technique'. Power Electronics Specialists Conf., 2004, PESC 04, 2004 IEEE 35th Annual, 2004, vol. 3, pp. 1945–1949

[4] KOUTROULIS E., KALAITZAKIS K., VOULGARIS N.C.: 'Development of a microcontroller-based, photovoltaic maximum power point tracking control system', *IEEE Trans. Power Electron.*, 2001, **16**, (1), pp. 46–54

[5] KISLOVSKI A.S.: 'Dynamic behavior of a constant-frequency buck converter power cell in a photovoltaic battery charger with a maximum power tracker'. Fifth Applied Power Electronics Conf. and Exposition, APEC, 1990

[6] VILLALVA M.G., GAZOLI J.R., RUPPERT E.F.: 'Analysis and simulation of the P&O MPPT algorithm using a linearized photovoltaic array model'. Tenth Brazilian Power Electronics Conf., COBEP, 2009

[7] Kyocera: 'KC200GT high efficiency multicrystal photovoltaic module datasheet', available at: http://www.kyocerasdar.com/pdf/specsheets/KC200GT.pdf

[8] VILLALVA M.G., GAZOLI J.R., RUPPERT E.F.: 'Comprehensive approach to modeling and simulation of photovoltaic arrays', *IEEE Trans. Power Electron.*, 2009, **25**, (5), pp. 1198–1208

[9] VILLALVA M.G., GAZOLI J.R., RUPPERT E.F.: 'Modeling and circuit-based simulation of photovoltaic arrays', *Revista Eletrônica de Potência (SOBRAEP), Brazilian J. Power Electron.*, 2009, **14**, pp. 35–45

[10] VILLALVA M.G., RUPPERT E.F.: 'Dynamic analysis of the input-controlled buck converter fed by a photovoltaic array', *Revista Controle & Automação – Sociedade Brasileira de Automática, Brazilian J. Control Autom.*, 2008, **19**, (4), pp. 463–474

[11] CUK S., MIDDLEBROOK R.D.: 'Modeling, analysis and design of switching converters'. Technical Report, California Institute of Technology, 1977

[12] MIDDLEBROOK R.D.: 'Small-signal modeling of pulse-width modulated switched-mode power converters', *Proc. IEEE*, 1988, **76**, (4), pp. 343–354

© The Institution of Engineering and Technology 2010

[13] MIDDLEBROOK R.D., CUK S.: 'A general unified approach to modelling switching converter power stage'. IEEE Power Electronics Specialists Conf., 1976, pp. 18–34

[14] ERICKSON R.W., MAKSIMOVIC D.: 'Fundamentals of power electronics' (Kluwer Academic Publishers, 2001)

[15] ZHIHAO Y., XIAOBO W.: 'Compensation loop design of a photovoltaic system based on constant voltage MPPT'. Power and Energy Engineering Conf., 2009, APPEEC 2009, Asia-Pacific, 27–31 March 2009, pp. 1–4

[16] FRANKLIN G.F., POWELL J.D., EMAMI-NAEINI A.: 'Feedback control of dynamic systems' (Prentice Hall, 2002, 4th edn.)

[17] OPPENHEIM A.V., SCHAFER R.W.: 'Discrete-time signal processing' (Prentice Hall, 1999, 2nd edn.)

© The Institution of Engineering and Technology 2010
doi: 10.1049/iet-pel.2008.0344